Giant Zero Bias Anomaly due to Coherent Scattering from Frozen Phonon Disorder in Quantum Point Contacts

Y.-H. Lee, S. Xiao, K. W. Kim, J. L. Reno, J. P. Bird, and J. E. Han

Phys. Rev. Lett. **123**, 056802 — Published 30 July 2019

DOI: 10.1103/PhysRevLett.123.056802

Giant Zero Bias Anomaly due to Coherent Scattering from Frozen Phonon Disorder in Quantum Point Contacts

Y.-H. Lee,[1] S. Xiao,[1] K. W. Kim,[2] J. L. Reno,[3] J. P. Bird,[1,*] and J. E. Han[4,†]

[1]*Department of Electrical Engineering, University at Buffalo, the State University of New York, Buffalo, New York 14260, USA*
[2]*School of Physics, Korea Institute for Advanced Study, Seoul 02455, Korea*
[3]*CINT, Sandia National Laboratories, Dept. 1131, MS 1303, Albuquerque, NM 87185, USA*
[4]*Department of Physics, University at Buffalo, the State University of New York, Buffalo, NY 14260, USA*

(Dated: July 8, 2019)

We demonstrate an unusual manifestation of coherent scattering for electron waves in mesoscopic quantum point contacts, in which fast electron dynamics allows the phonon system to serve as a quasi-static source of disorder. The low-temperature conductance of these devices exhibits a giant ($\gg 2e^2/h$) zero-bias anomaly (ZBA), the features of which are reproduced in a nonequilibrium model for coherent scattering from the "frozen" phonon disorder. According to this model, the ZBA is understood to result from the *in situ* electrical manipulation of the phonon disorder, a mechanism that could open up a pathway to the on-demand control of coherent scattering in the solid-state.

PACS numbers: 73.21.Hb, 73.23.Ad, 73.63.Nm, 71.10.Pm

The coherent scattering of propagating waves has long been studied in the literature, in the context of both classical and quantum transport. Examples include strong [1–6] and weak [7–10] localization, and universal conductance fluctuations [11, 12]. In this work, we demonstrate an unusual manifestation of coherent electron scattering, in the low-temperature electron transport through quantum point contacts (QPCs, see Figs. 1). These devices are characterized by a low level of structural (impurity- or defect-related) disorder, which allows us to access a regime in which phonon excitation functions as a controlled source of disorder. We show here how the phonon induced lattice distortion that is the source of this disorder may be manipulated via the ambient temperature, and by the size of the bias applied to generate transport through the device. The temperature determines the amplitude of the disorder at thermal equilibrium, while the bias allows drifting electrons to stochastically impart energy and momentum to the crystal lattice, thereby leading to the emergence of different disorder behaviors. These concepts are applied to account for a remarkable feature in the QPCs, namely a giant zero-bias anomaly (ZBA) in their differential conductance [$g_d(V_d) = dI/dV_d$, where V_d is the applied source-drain bias, and I the electrical current]. The anomaly is characterized by a precipitous drop of conductance, as either the temperature or bias is increased, behavior that we reproduce with nonequilibrium transport calculations. These attribute the anomaly to a coherent scattering process involving multiple quantum channels (or subbands), in a manner that may be controlled directly via the bias and/or temperature.

The QPCs [13, 14] we study were formed in the two-dimensional electron gas (2DEG) of a GaAs/AlGaAs heterostructure [see Sec. S1 of the Supplemental Material (SM) [15] for further details]. At low temperatures, the superposition of thermally-activated acoustic phonons generates a stochastic variation of the crystal lattice, which may in turn be viewed as a random contribution to the confining potential of the QPC (see Fig. 1(b)). Crucial here is the slow dynamics of this contribution, a point that may be made by using the equipartition concept to determine the characteristic time scale ($\tau_{\rm ph}$) of phonon motion. Equating the phonon energy ($h/\tau_{\rm ph}$) to the thermal energy ($\frac{1}{2}k_BT$, where k_B is the Boltzmann constant), we obtain $\tau_{\rm ph} = 2h/k_BT$. At a representative temperature of 10 K this scale is around 10 ps, longer than the time needed for electrons to transit through the QPC. Taking account of the depth of the 2DEG layer, and assuming an effective QPC length of 500 nm (and a Fermi velocity of 2×10^5 ms^{-1}), for example, the transit time ($\tau_{\rm tr} \sim L/v_F$, where v_F is the Fermi velocity and L is the QPC length) should be no more than a few $(2 - 3)$ ps. In other words, for temperatures close to, or lower than, this value, the frozen-phonon concept should be valid and individual electrons transitioning through the QPC will observe quasi-static atomic disorder, arising from the instantaneous distortion of the crystal lattice by the phonons. At higher temperatures, as the phonon period decreases, this criterion will no longer be met for electrons as they transition across the full device. Nonetheless, there should still be significant sections, connected in series with one another, inside each of which the frozen-phonon concept should be valid [11].

The spatial scale of lattice distortion generated by the phonon motions may be estimated from the thermal wavelength of the acoustic modes ($\lambda_{\rm ph} = v_s\tau_{\rm ph} = hv_s/k_BT$). Here, v_s is the sound velocity, which we take to be 4000 ms^{-1} for the (001) surface of GaAs. In this way we obtain $\lambda_{\rm ph} \sim 20$ nm at 10 K, implying multiple scattering within the QPC ($\lambda_{\rm ph} < L$). Since the scatter-

ing length $\lambda_{\rm ph}$ increases at lower temperatures, we expect coherent scattering from the frozen disorder to be effective over a specific range of temperature, which should be high enough to ensure that $L/\lambda_{\rm ph} > 1$, yet low enough to satisfy the frozen-disorder approximation ($\tau_{\rm ph} > \tau_{\rm tr}$). For a more detailed discussion of these points we refer the reader to Sec. S2 of the SM, where evidence for these regimes is found in measurements made down to mK temperatures.

The implications of coherent scattering in one-dimensional transport were considered in the seminal work of Landauer [16, 17]. Extending his findings to a quasi-one-dimensional conductor of length L, whose carriers are scattered by static impurities on a length scale L_n (where the subscript denotes the n^{th} transport mode), the conductance decays as:

$$g_d(L) \approx \sum_n e^{-L/L_n}. \qquad (1)$$

In this work, we explicitly demonstrate (in experiment and theory) a ZBA with such strong conductance scaling, and argue that it arises from the coherent scattering generated by the frozen displacements of the lattice, which strongly mix the (originally ballistic) 1D subbands into decaying transport modes with short L_n.

In contrast to prior works that have explored the quantized conductance of QPCs at very low temperatures [14, 18, 19], in this Letter we focus on the behavior observed at higher temperatures, where the frozen lattice displacements generated by the phonons give rise to considerable inter-subband scattering. Our experiments make use of heterostructures whose 2DEG lies far (more than 500 nm, see Sec. S1 of the SM) below the surface gates. This results in weaker lateral confinement of carriers than is common in typical experiments, consistent with which we note that the usual 1D conductance quantization is only clearly manifested for the lowest-order plateaus in our devices. This can be seen in the right inset to Fig. 1(a), which plots the low temperature (20 mK) linear conductance [$G \equiv g_d(V_d = 0)$] of one of our QPCs, as a function of its gate voltage (V_g). While clear plateaus are present at 0.7 and $1 \times 2e^2/h$ [14], opening the QPC up to increase conduction rapidly suppresses the higher plateaus. Similarly, the quantization is suppressed quickly with increase of temperature, being absent completely for the range (4.2 K $< T <$ 40 K) over which we focus in this study.

The ZBA of interest here is presented in Fig. 1(a), which shows the low-temperature differential conductance of one of our QPCs at various gate voltages. The ZBA corresponds to the dramatic drop in conductance that is observed for drain biases of just a few mV. Dependent upon the initial conductance, the anomaly can be several multiples of the basic conductance quantum ($G_0 = 2e^2/h$) in size, indicating it arises from scattering

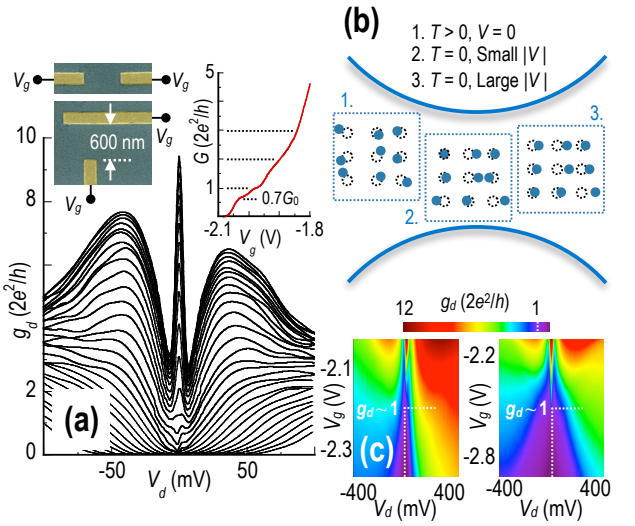

FIG. 1: (a) Differential conductance of a QPC with asymmetric gate geometry at 4.2 K. Gate voltage is varied in 20-mV increments from −1.82 V (top) to −2.36 V (bottom). The left insets are scanning-electron micrographs of symmetric (top) and asymmetric QPCs. The right inset shows the quantized conductance in a typical QPC at 20 mK. (b) Schematic representation of three different frozen-phonon realizations (labeled in figure). These "snapshots" of the lattice vibration schematically denote the instantaneous displacement of GaAs atoms from their equilibrium positions. (c) Contour plots showing the variation of differential conductance for an asymmetric (left panel) and asymmetric (right panel) QPC.

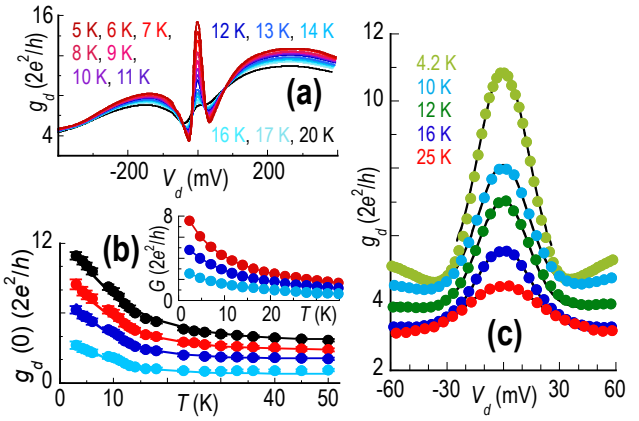

FIG. 2: (a) Temperature dependence of the ZBA in an asymmetric QPC at fixed gate voltage. (b) Temperature dependence of the zero-bias conductance of the device of (a) at different gate conditions. The solid lines are fits to $g_d(V_d = 0, T) = g_{0,T} + \Delta g_T e^{-T/T_0}$, where T_0 varies from 10.4- to 7.4-K, from top to bottom, respectively. The inset shows corresponding theoretical calculations with a chemical potential in the QPC of 10 meV (red), 6 meV (blue) and 3 meV (cyan). (c) The voltage dependence of ZBA of a symmetric QPC at different temperatures. Only a fraction of data are shown and solid lines are fits to $g_d(V_d) = g_{0,V_d} + \Delta g_{V_d} e^{-(V_d/V_0)^2}$, V_0 ranges from 19- to 25-mV, from lowest to highest temperature, respectively.

induced within multiple subbands. This is to be contrasted with more-widely studied forms of ZBA, such as those associated with Kondo [20–22] and Majorana [23–25] physics, which are attributed to many-body effects in the lowest subband and whose size is usually smaller than G_0.

In Fig. 1(c) we demonstrate that that the ZBA is present for QPCs with both symmetric and asymmetric gate configurations (see the upper-left insets of Fig. 1(a)), indicating that this feature is intrinsic to nonequilibrium transport, regardless of the precise potential profile of the devices. The anomaly is followed by a sudden crossover to the opposite behavior at nonzero bias, with the differential conductance now increasing with further increase of the voltage. Importantly for the formulation of our model, both the ZBA, and the subsequent recovery of conductance, occur at voltages below those for which the excitation of optical phonons is expected to be significant in GaAs [26–28].

In Fig. 2(a) we present another example of the ZBA, showing how it is strongly damped with increase of temperature above 4 K. Reflecting this, the temperature dependence of the zero-bias conductance $[g_d(V_d = 0, T)]$ is plotted (for four gate voltages) in Fig. 2(b), and decreases by several multiples of G_0 when the temperature is raised to 50 K. While this very large conductance change is uncharacteristic of typical mesoscopic phenomena, and occurs over a range for which the 2DEG conductivity is virtually independent of temperature [29], it does appear consistent with the exponential decay of Eq. (1), as indicated by the solid lines through the data. These follow the form $g_d(V_d = 0, T) \propto e^{-T/T_0}$, where T_0 is an effective temperature.

The voltage-dependent lineshape of the ZBA [see Fig. 2(c)] is also consistent with an exponential scaling, which in this case varies as $g_d(V_d) \propto e^{-(V_d/V_0)^2}$ (where V_0 is a characteristic voltage scale). Important to note here are the different functional forms of the temperature and voltage scaling, and the fact that $eV_0 \gg k_B T_0$. These characteristics suggest that a simple interpretation of the influence of the drain voltage in terms of equivalent heating is not appropriate.

To formulate a theoretical description of our results, we begin from a simple, heuristic argument. Within the frozen-phonon model, lattice disorder arises from the excitation of long-wavelength acoustic phonons, which generate random "strain" $[\vec{\varphi}(\mathbf{r})]$ in the crystal on a scale $(\sim \lambda_{\rm ph})$ much longer than the interatomic spacing. There are two contributions to this strain: (i) random and isotropic phonon excitations at thermal equilibrium (Fig. 1(b), left panel), and; (ii) nonequilibrium excitations under bias, arising from the continuous transfer of energy and momentum from drifting electrons to the lattice. At steady-state, this transfer maintains a rigid shift of the Fermi sphere, and imparts linear momentum from electrons to phonons, thereby causing the lattice disorder to

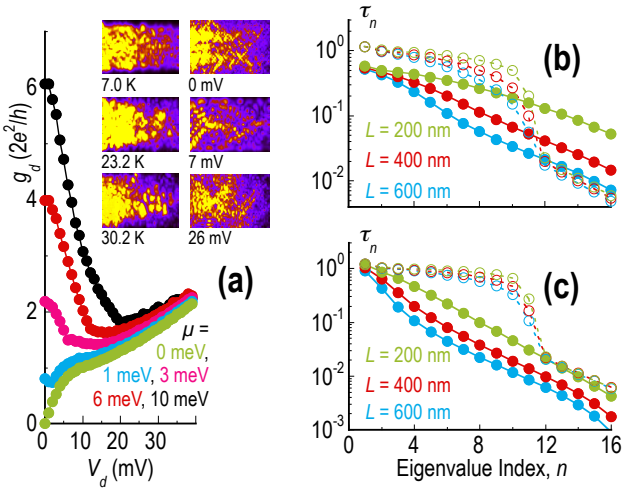

FIG. 3: (a) Computed differential conductance at different chemical potentials. The insets are maps of the electron density originating from the source lead at $\mu = 6$ meV, and at the indicated temperatures (left column, $V_d = 0$) and biases (right column, $T = 4$ K). At $V_d = 25$ mV, recovery of the wavefunction amplitude is evident in the bottom-right panel. (b) and (c) Eigenvalues of the transmission matrix and their dependence on bias and temperature, respectively ($\mu = 10$ meV, $\Delta = 1$ meV). In (b), open (closed) symbols are for $V_d = 0$ (20) mV while in (c) open (closed) symbols are for $T = 2.3$ (23) K.

develop a directional character, along the axis defined by the bias (as indicated in the center and right panels of Fig. 1(b)). In a certain sense, this may be thought of as the inverse of the phonon-drag effect that has previously been demonstrated in 2DEG systems [30]. To appreciate how the application of even a small (mV) bias voltage may give rise to significant disorder, we note that the corresponding electric field it gives rise to is in the range of kV/cm.

In a tight-binding description of electron transport, the lattice displacement $\vec{\varphi}(\mathbf{r})$ modifies electron hopping and serves as a source of scattering. In the case where temperature alone is varied, the induced displacement may be estimated in the equipartition limit by equating the thermal energy $(\propto k_B T)$ to the lattice elastic energy $(\propto |\vec{\varphi}|^2)$. This gives $|\vec{\varphi}| \propto \sqrt{T}$, which, when introduced into Fermi's golden rule, yields a scattering rate proportional to $|\vec{\varphi}|^2$. Relating this rate to a corresponding scattering length $L_n(T, V_d = 0) \propto 1/|\vec{\varphi}|^2 \propto 1/T$, we then use Eq. (1) to arrive at the temperature-dependent conductance, $g_d(V_d = 0, T) \propto e^{-T/T_0}$. This dependence is in good agreement with what we observe in experiment, as shown in Fig. 2(b).

In contrast to the effect of temperature, the applied bias will generate two forms of lattice displacement [see Fig. 1(b), center panel]: (i) a uniform shift due to net momentum transfer, superimposed upon which is; (ii) a

random term that reflects the stochastic nature of the electron-phonon scattering. The random component is estimated by relating the elastic energy to the electrical power ($\propto V_d^2$), dissipated during the approach to steady-state. [Note that the time required to reach this nonequilibrium state should be much longer than the electron transit time ($\tau_{\rm tr}$) through the QPC. Furthermore, the accumulated effects of this dissipation will not be limited to the immediate vicinity of the QPC, but will extend, also, into the reservoirs.] Following similar steps to those above, we obtain $L_n(T \approx 0, V_d) \propto V_d^{-2}$ and a corresponding differential conductance $g_d(T \approx 0, V_d) \propto e^{-(V_d/V_0)^2}$. Once again, this form is consistent with experiment, as shown in Fig. 2(c).

The heuristic arguments above motivate the development of a quantitative model of nonequilibrium transport in QPCs, subject to a random potential that is controlled by temperature and bias. This problem is discretized on a square grid, with a lattice spacing ($a = 10$ nm) that is comparable to the phonon wavelength ($\lambda_{\rm ph} \sim 20$ nm) at 10 K. The in-plane displacement within each cell of this grid is then expressed as:

$$\frac{\vec{\varphi}(\mathbf{r})}{a} = \alpha \left(\frac{k_B T}{\epsilon_0}\right)^{1/2} \vec{u}(\mathbf{r}) + \left(\frac{eV_d}{\epsilon_0}\right) [\beta_1 + \beta_2 v(\mathbf{r})]\hat{\mathbf{x}}, \quad (2)$$

where the energy unit $\epsilon_0 = 1$ meV, $\vec{u}(\mathbf{r})$ is a random vector with magnitude in the range $[0, 1]$, $v(\mathbf{r})$ is a random number in the range $[-1, 1]$, and $\hat{\mathbf{x}}$ is the unit vector along the applied electric field. For the purpose of calculation, the coefficient α that governs the temperature-dependent term in this equation was estimated from the 2DEG mobility, yielding $\alpha = 0.015$. (We refer the reader to Sec. S3 of the SM for details of our model, and a discussion of its equivalence to conventional scattering theory [31–33] and the theory of elasticity [34]). The coefficients β_1 and β_2 define the static and random displacements due to the bias, respectively, and, while little is known about their values *a priori*, we assume that they are both smaller than α. As justification for this, we note that the process by which the bias-induced displacements are generated should be less effective than that responsible for the thermally-driven ones.

Kawamura and Das Sarma [35] have studied the rate of electron scattering by acoustic phonons in a 2DEG, demonstrating a saturation for electron energies beyond the Fermi level. Motivated by this, we impose an upper bound ($\Delta a_m \equiv |\vec{\varphi}|_{\rm max}$) on the bias-induced displacements, which we set at 3% of the discretization spacing a (see Sec. S3.2 of the SM for a more detailed justification). We impose this bound via the mapping:

$$\vec{\varphi} \mapsto \Delta a_m \hat{\mathbf{e}}_\varphi \tanh \frac{|\vec{\varphi}|}{\Delta a_m}, \quad (3)$$

with the unit vector $\hat{\mathbf{e}}_\varphi \parallel \vec{\varphi}$. The hyperbolic tangent in this phenomenological expression yields the correct behavior for the temperature- and bias-dependent displacements, including their required saturation at larger values of these parameters. Of particular interest is the case of large voltage, for which the displacements develop a strong alignment along the field direction, implying that the phonon-induced disorder has been (at least partially) lifted [see Fig. 1(b), right panel]. It is this effect that we attribute to the restoration of conductance at nonzero bias, seen in the experiments.

To calculate the differential conductance within our model, we use nonequilibrium Green's function method, with the hopping disorder generated by the displacements in Eqs. (2) and (3) (see the SM for further details). In Fig. 3(a), we plot this conductance for four different values of the chemical potential (equivalent to different gate voltages), after averaging over 500 random disorder configurations. In spite of the microscopic simplicity of our model, the calculations reproduce the giant ZBA (with amplitude much larger than G_0) and the recovery of conductance at higher voltages. Another feature of the experiment that is reproduced is the suppression of the anomaly as the zero-bias conductance is reduced towards $2e^2/h$ (compare Figs. 1(a) & 3(a)). This behavior arises from the fact that the phase-space for elastic intersubband scattering, responsible for the ZBA, is dramatically reduced as the last subband is depopulated.

Using parameters that are consistent with the literature (see the SM), and with the experimentally-measured mobility, our calculations demonstrate that the ZBA arises from coherent scattering generated by the bias-controlled lattice displacements. In the inset to Fig. 2(b), we show that the calculated temperature dependence of the zero-bias conductance is consistent with the corresponding experimental variations. An important question that arises here concerns the extent to which these variations arise from a coherent, as opposed to an incoherent, scattering effect. To address this issue, we note that the temperature-dependent variation of the zero-bias conductance is stronger (in both experiment and theory) than one would expect for an incoherent effect. To establish this point, we may perturbatively compute the conductance variation expected in our model in the presence of incoherent scattering. For a zero-bias displacement defined according to Eq. 2, this yields a scattering rate (see Eq. S10 of the SM), and thus a zero-bias resistance, that varies linearly in T. As we demonstrate in Sec. S3.2 of the SM, the linear dependence is slower than that which arises when accounting for coherence in transport.

In Figs. 3(b) & 3(c) we plot the eigenvalues of the transmission matrix (τ_n, see Sec. S3.4 of the SM), which describe the quantum-mechanical overlap of the source and drain through the n^{th} transport mode. In the limit of either low temperature or bias (open symbols), where the disorder is minimized, the eigenvalues show the usual quasiballistic crossover from strongly trans-

mitted ($\tau_n \sim 1$) to heavily reflected ($\tau_n \ll 1$) modes, once $n > \mu/\Delta$ (where μ is the chemical potential inside the QPC, and Δ is the subband spacing). At elevated temperature or bias, however, the increased disorder generated by the lattice displacements suppresses this crossover and the eigenvalues instead show a tendency for exponential decay, behavior that is reminiscent of the influence of localization [36]. The lack of any clear crossover in this case, from transmitted to reflected modes, points to strong mixing of the original subbands of the QPC. Also important in this regime is that the eigenvalue transmission for all modes shows a scaling (i.e. a slope) that is close to that of the original evanescent ones.

The electron density originating from the source is calculated for a single (unaveraged) disorder configuration in Fig. 3(a). The left column shows the influence of increasing temperature, and reflects the corresponding growth of the phonon-driven disorder. The right column, on the other hand, captures the effect of the drain voltage, and shows a clear signature of conductance recovery at the largest bias that is consistent with the "restoration" of order described by Eq. (3).

In conclusion, we have demonstrated a giant ZBA in QPCs, arising from coherent scattering of electron waves in the presence of frozen phonon disorder. Comparison of our experiment with the results of a nonequilibrium model reveals how transmission of the quasiballistic QPC subbands is progressively suppressed, as the phonon disorder is increased via thermal or electrical control. In the latter case, application of the drain bias first causes a ZBA, which is followed by a partial recovery of conductance at larger bias due to a "restoration" of lattice order. These observations arise from the interference of electron waves that undergo multiple scattering from the phonon disorder. Our results should be broadly applicable to other nanoscale conductors, including molecular wires, nanotubes and metallic nanojunctions.

The experimental work here was supported by the U.S. Department of Energy, Office of Basic Energy Sciences, Division of Materials Sciences and Engineering under Award DE-FG02-04ER46180. JEH acknowledges the computational support from the CCR at University at Buffalo.

* Electronic address: jbird@buffalo.edu
† Electronic address: jonghan@buffalo.edu

[1] P. W. Anderson, Phys. Rev. **109**, 1492 (1958).
[2] S. Longhi, Laser & Photon. Rev. **3**, 243 (2009).
[3] D. S. Wiersma, Nat. Photonics **7**, 188 (2013).
[4] M. Segev, Y. Silberberg, and D. N. Christodoulides, Nat. Photonics **7**, 197 (2013).
[5] J. Billy, V. Josse, Z. Zuo, A. Bernard, B. Hambrecht, P. Lugan, D. Clement, L. Sanchez-Palencia, P. Bouyer, and A. Aspect, Nature **453**, 891 (2008).
[6] G. Roati, C. D'Errico, L. Fallani, M. Fattori, C. Fort, M. Zaccanti, G. Modugno, M. Modugno, and M. Inguscio, Nature **453**, 895 (2008).
[7] G. Bergmann, Phys. Rev. B **28**, 2914 (1983).
[8] G. Bergmann, Phys. Rep. **107**, 1 (1984).
[9] P. A. Lee and T. V. Ramakrishnan, Rev. Mod. Phys. **57**, 287 (1985).
[10] B. L. Altshuler, A. G. Aronov, and P. A. Lee, Phys. Rev. Lett. **44**, 1288 (1980).
[11] P. A. Lee, A. D. Stone, and H. Fukuyama, Phys. Rev. B **35**, 1039 (1987).
[12] S. Washburn and R. Webb, Adv. Phys. **35**, 375 (1986).
[13] See Ch. 5 of D. K. Ferry, S. M. Goodnick, and J. P. Bird, *Transport in Nanostructures* (Cambridge Univ. Press, Cambridge, 2009).
[14] A. P. Micolich, J. Phys.: Cond. Matt. **23**, 443201 (2011).
[15] See Supplemental Material [url] for information on device fabrication, low temperature data, and model construction, which includes Refs. [31–34].
[16] R. Landauer, Philos. Mag. **21**, 863 (1970).
[17] See Ch. 5 of S. Datta, *Electronic Transport in Mesoscopic Systems* (Cambridge Univ. Press, Cambridge, 1995).
[18] D. A. Wharam, T. J. Thornton, R. Newbury, M. Pepper, H. Ahmed, J. E. F. Frost, D. G. Hasko, D. C. Peacock, D. A. Ritchie, and G. A. C. Jones, J. Phys. C: Solid State Phys. **21** L209 (1988).
[19] B. J. van Wees, H. van Houten, C. W. J. Beenakker, J. G. Williamson, L. P. Kouwenhoven, D. van der Marel, and C. T. Foxon, Phys. Rev. Lett. **60**, 848 (1988).
[20] W. G. van der Wiel, S. De Franceschi, T. Fujisawa, J. M. Elzerman, S. Tarucha, and L. P. Kouwenhoven, Science **289**, 2105 (2000).
[21] D. Goldhaber-Gordon, J. Göres, M. A. Kastner, H. Shtrikman, D. Mahalu, and U. Meirav, Phys. Rev. Lett. **81**, 5225 (2003).
[22] S. M. Cronenwett, H. J. Lynch, D. Goldhaber-Gordon, L. P. Kouwenhoven, C. M. Marcus, K. Hirose, N. S. Wingreen, and V. Umansky, Phys. Rev. Lett. **88**, 226805 (2003).
[23] V. Mourik, K. Zuo, S. M. Frolov, S. Plissard, E. P. A. M. Bakkers, and L. P. Kouwenhoven, Science **336**, 1003 (2012).
[24] M. T. Deng, C. L. Yu, G. Y. Huang, M. Larsson, P. Caroff, and H. Q. Xu, Nano Lett. **12**, 6414 (2012).
[25] A. Das, Y. Ronen, Y. Most, Y. Oreg, M. Heiblum, and H. Shtrikman, Nat. Phys. **8**, 887 (2012).
[26] U. Sivan, M. Heiblum, and C. P. Umbach, Phys. Rev. Lett. **63**, 992 (1989).
[27] A. S. Dzurak, C. J. B. Ford, M. J. Kelly, M. Pepper, J. E. F. Frost, D. A. Ritchie, G. A. C. Jones, H. Ahmed, and D. G. Hasko, Phys. Rev. B **45**, 6309 (1992).
[28] G. J. Schinner, H. P. Tranitz, W. Wegscheider, J. P. Kotthaus, S. Ludwig, Phys. Rev. Lett. **102**, 186801 (2009).
[29] N. A. Kabir, Y. Yoon, J. R. Knab, J.-Y. Chen, A. G. Markelz, J. L. Reno, Y. Sadofyev, S. Johnson, Y.-H. Zhang, and J. P. Bird, Appl. Phys. Lett. **89**, 132109 (2006).
[30] H. Karl, W. Dietsche, A. Fischer, and K. Ploog, Phys. Rev. Lett. **61**, 2360 (1988).
[31] J. M. Ziman, *Principles of the Theory of Solids*, 2nd Ed., p. 205 (Cambridge, UK, 1972)
[32] David K. Ferry, *Semiconductors*, p. 212-215 (McMillan, USA, 1991).

[33] G. Mahan, *Many-Particle Physics* (Plenum Press. USA, 1981).
[34] J. L. Martins and A. Zunger, Phys. Rev. B **30**, 6217 (1984).
[35] T. Kawamura, and S. Das Sarma, Phys. Rev. B **45**, 3612 (1992).
[36] To represent the influence of the diffusive (i.e. nearly-transmitted) modes for small index n (for which $\tau_n \lesssim 1$), Eq. (1) may be expressed in the form $g_0 + \sum' e^{-L/L_n}$, where the summation now excludes the diffusive modes. Introducing g_0 in this manner provides a justification for the fixed-conductance term used in the experimental fits in Fig. 2.